

# Journal of Biomedical Optics

BiomedicalOptics.SPIEDigitalLibrary.org

## **Simulated altitude exposure assessment by hyperspectral imaging**

Mihaela Antonina Calin  
Adrian Macovei  
Sorin Miclos  
Sorin Viorel Parasca  
Roxana Savastru  
Razvan Hristea

# Simulated altitude exposure assessment by hyperspectral imaging

Mihaela Antonina Calin,<sup>a,\*</sup> Adrian Macovei,<sup>b</sup> Sorin Miclos,<sup>a</sup> Sorin Viorel Parasca,<sup>c,d</sup> Roxana Savastru,<sup>a</sup> and Razvan Hristea<sup>b</sup>

<sup>a</sup>National Institute of Research and Development for Optoelectronics—INOE 2000, Magurele, Romania

<sup>b</sup>National Institute of Aeronautical and Space Medicine, “Gen. Dr. Aviator Victor Anastasiu,” Bucharest, Romania

<sup>c</sup>Emergency Clinical Hospital for Plastic, Reconstructive Surgery and Burns, Bucharest, Romania

<sup>d</sup>Carol Davila University of Medicine and Pharmacy, Department of Plastic and Reconstructive Surgery, Bucharest, Romania

**Abstract.** Testing the human body’s reaction to hypoxia (including the one generated by high altitude) is important in aeronautic medicine. This paper presents a method of monitoring blood oxygenation during experimental hypoxia using hyperspectral imaging (HSI) and a spectral unmixing model based on a modified Beer–Lambert law. A total of 20 healthy volunteers (males) aged 25 to 60 years were included in this study. A line-scan HSI system was used to acquire images of the faces of the subjects. The method generated oxyhemoglobin and deoxyhemoglobin distribution maps from the foreheads of the subjects at 5 and 10 min of hypoxia and after recovery in a high oxygen breathing mixture. The method also generated oxygen saturation maps that were validated using pulse oximetry. An interesting pattern of desaturation on the forehead was discovered during the study, showing one of the advantages of using HSI for skin oxygenation monitoring in hypoxic conditions. This could bring new insight into the physiological response to high altitude and may become a step forward in air crew testing. © 2017 Society of Photo-Optical Instrumentation Engineers (SPIE) [DOI: 10.1117/1.JBO.22.5.056012]

Keywords: altitude hypoxia; tissue oxygenation; oxyhemoglobin; deoxyhemoglobin; oxygen saturation; hyperspectral imaging.

Paper 170050R received Jan. 20, 2017; accepted for publication May 16, 2017; published online May 31, 2017.

## 1 Introduction

Hypoxia is a well-known medical condition in which insufficient amounts of oxygen are available to cells. It can be caused by different conditions:<sup>1</sup> the partial pressure of oxygen in the inspired air is reduced beyond possible human physiological compatibility (hypoxic hypoxia type, also called altitude hypoxia), the capacity of blood to carry oxygen is reduced due to decreased hemoglobin content (anemic hypoxia type), an inadequate circulation of the blood exists even if the oxygen carrying capacity of the blood is adequate (stagnant hypoxia type), and the cells are unable to take up or utilize oxygen from the blood due to tissue poisoning by certain toxic chemical compounds such as cyanide or hydrogen sulfide (histotoxic hypoxia type).

Various types of hypoxia may be encountered in military pilots (the flight crew), but the most frequent and important of them is hypoxic hypoxia induced by the decrease of the partial pressure of oxygen in the inspired air with increasing altitude.<sup>2</sup> At high altitude, the difference between the pressure of oxygen in the inspired air in the lungs and the pressure of the oxygen in the blood, tissues, or cells can reach low values, preventing hemoglobin from binding to oxygen and, thus, negatively affecting the efficient transport of oxygen.

Despite the technological advances made in the military aviation field, such as improvements in oxygen delivery systems and the extensive physiology training, hypoxia remains an undesired medical condition still encountered by military pilots. Therefore, the key challenges for specialists are the expansion of basic, scientific, and technical approaches toward innovative technical solutions for more reliable cabin pressurization, the

development of advanced oxygen delivery systems, a better understanding of the molecular/cellular mechanisms of hypoxia and its physiological effects, the development of efficient systems for monitoring tissue oxygenation, and the early detection of hypoxia.

It is well known that the most common ways to detect hypoxia are the examination of physical signs (dyspnea, tachycardia, and paresthesia) and individual symptoms (nausea, light-headedness, visual impairment, dizziness, and impairment of cognitive function)<sup>3</sup> and the monitoring of pulse rate and peripheral oxygen saturation using a pulse oximeter.<sup>4</sup> Both methods, however, have limitations. Hypoxia signs and symptoms may vary among individuals and are useful for training but are less useful as a monitoring method.<sup>5</sup> Pulse oximetry allows the noninvasive and continuous monitoring of peripheral oxygen saturation, but it has low accuracy at extremely low levels of oxygen saturation (below 70%).<sup>6</sup> In this paper, we propose an approach for assessing hypoxia based on hyperspectral imaging (HSI). HSI consists of recording a set of images (tens or hundreds of images) for every time point in many adjacent narrow spectral bands (typically between 2 to 4 nm) and reconstructing the reflectance spectrum for every pixel of the image.<sup>7</sup> Using this spatial and spectral information, the tissue constituents can be identified from the reflectance spectrum of each image pixel based on their spectral signature. In addition, the relative concentration of these constitutive elements may be also determined using appropriate statistical analysis methods.<sup>8</sup> “This technique is a relatively new optical method for the medical field with large possibilities for application in the detection of cancer, diabetic foot ulcer prognosis, peripheral vascular disease assessment, etc.”<sup>9</sup>

\*Address all correspondence to: Mihaela Antonina Calin, E-mail: [mantonina\\_calin@yahoo.com](mailto:mantonina_calin@yahoo.com)

The aim of this study was to test the ability of HSI technique together with some image processing and analysis methods to provide information about tissue oxygenation during induced hypoxia in voluntary subjects. This information is very useful for creating an individualized physiological profile on hypoxia exposure.

The analyses were mainly focused on: (a) establishing the experimental conditions for hyperspectral images acquisition; (b) identifying the most appropriate methods for hyperspectral image processing; (c) selecting an appropriate method for hyperspectral image analysis having maps of the oxyhemoglobin, deoxyhemoglobin, and oxygen saturation as the results; and (d) demonstrating the HSI technique efficacy as method of hypoxia assessment by comparison with standard pulse-oximetry measurements.

## 2 Materials and Methods

### 2.1 Subjects

Twenty healthy volunteers (males, aged 25 and 60 years) were included in this study (Table 1).

The subjects were screened for any pathology or anomalies regarding cardiac, pulmonary, and neurological functions. Subjects positive for any of the screened anomalies were excluded. Informed consent was obtained from each subject prior to participation in this study.

The subjects were selected by voluntary decision of inclusion (aviation military personnel). The subjects were picked following their yearly medical checkup, which included internal medicine, surgery, ear, nose, and throat, ophthalmology, neurology, and psychiatry, as well as pulmonary Rx, electrocardiogram, and a full panel blood test. All subjects were declared fit. Approval for all procedures and the use of human subjects was obtained from the Ethics Committee of the “Gen. Dr. Aviator Victor Anastasiu” National Institute of Aeronautical and Space Medicine.

### 2.2 Altitude Exposure Simulation Procedure

Each subject was individually exposed to a simulated altitude of 7620 m, a common altitude used in training profiles of military personnel, chosen according to the recommendation of the manual and software of the reduced-oxygen breathing device (GO2Altitude Hypoxia Training System ver 2.0, London, UK), a medical grade device certified for human use. The system belongs to the professional devices category, but it was designed specifically for military training and it was customized. This system separates oxygen and nitrogen from air and stores them

in separate recipients; then, a computer mixes the gases according to the desired altitude (6% to 15%  $\pm$  0.5% oxygen in breathing air, to simulate altitudes of 35,000 to 8000 ft). The breathing device is a self-held mask. The mask was not attached due to safety concerns. Each subject was advised and checked for close mask fitness and proper operation. The system has an attached pulse oximeter for the continuous monitoring of peripheral arterial oxygen saturation.

The subjects were exposed to a simulated altitude equivalent to 7620 m, in one intermediate step (3500 m) from the ground level. The intermediate step at 3500 m is a producer safety measure to prevent sudden loss of consciousness due to exposure to abrupt hypoxia. Once the target altitude was reached, hyperspectral acquisition started. The experiment could be ended at any time using a kill switch, and, after exposure, recovery was made with oxygen of over 95% purity.

### 2.3 Hyperspectral Image Acquisition and Calibration

Hyperspectral images of the face of each subject were acquired at different moments during normobaric hypoxia at 7620 m equivalent to the beginning (0 min), middle (5 min), and end of testing (10 min) as well as at 10 min after oxygen recovery.

A line-scan HSI system mainly consisting of an HSI unit, an illumination unit containing two 300-W halogen lamps (OSRAM, Germany) equipped with diffusion filters (Kaiser Fototechnik GmbH & Co.KG, Buchen, Germany); a computer (CPU I7-4720HQ, 3.6 GHz, memory 16 GB, GPU GeForce GTX980M, Dell); a tripod (Manfrotto 055XDB, Cassola, Italy) with a mobile tripod head (Manfrotto MVH502AH); and image acquisition, processing, and analysis software (SpectralDAQ—Specim, Oulu, Finland and ENVI v.5.1—Exelis Visual Information Solutions, Boulder, Colorado) was used for hyperspectral image acquisition.

The hyperspectral image unit (PS-FW-11-V8E-OEM, Specim, Oulu, Finland) combines an imaging spectrometer (ImSpector V8E, Specim, Oulu, Finland, spectral range: 380 to 800 nm, spectral resolution: 2 nm, spectral sampling: 0.48 to 3.86 nm/pixel) equipped with a 19-deg field of view Xenoplan1.4/17 lens (Schneider, Bad Kreuznach, Germany) with a DX4 CCD camera (Kappa, Gleichen, Germany, resolution: 1392  $\times$  1040 pixels, pixel size: 6.45  $\mu$ m  $\times$  6.45  $\mu$ m, 42 frames/s at 4  $\times$  4 binning, firewire link). The unit acquires by its own software the hyperspectral data (as a hypercube) and sends them to the computer (via Firewire link) as an ENVI format file (.raw and .hdr files). This is a standard file format that can be opened by ENVI software and by our MATLAB software.

The breathing device was turned on at the beginning of the experiment, together with the hyperspectral unit and pulse oximeter. After data were acquired, the hyperspectral unit and pulse oximeter were turned off for 5 min; then they acquired new data and then were turned off again. The procedure was repeated at 10 min and once again at the end of the measurements. Each time the hyperspectral unit and the pulse oximeter were started simultaneously, but they were not synchronized.

The hyperspectral images acquired with this system can be influenced by both the inherent spatial nonuniformity of the artificial light intensity on the scene and the dark current in the CCD camera.<sup>10</sup> Therefore, all hyperspectral images were calibrated with white and dark reference images using<sup>11</sup>

$$I_{\text{calibrated}} = \frac{I_{\text{subject}} - I_{\text{dark}}}{I_{\text{white}} - I_{\text{dark}}}, \quad (1)$$

**Table 1** Patients selection by age, frequency, and percentage.

Age (years)	Frequency	Percentage (%)
20 to 30	7	35
30 to 40	7	35
40 to 50	5	25
50 to 60	1	5
Total	20	100

where  $I_{\text{calibrated}}$  is the calibrated hyperspectral image of the subject,  $I_{\text{subject}}$  is the original hyperspectral image of the subject,  $I_{\text{dark}}$  is the dark reference image obtained by completely covering the system lens, and  $I_{\text{white}}$  is the white reference image of a white polytetrafluoroethylene reference tile (model WS-2, Avantes, Apeldoorn, Netherlands) with  $\sim 98\%$  reflectance in spectral range 350 to 1800 nm located on the subject's chest (fixed with adhesive tape), having the same illumination conditions as the subjects. All the calibrated hyperspectral images were considered a basis for the subsequent assessment of hypoxia evolution in the subjects.

## 2.4 Hyperspectral Image Processing

A calibrated hyperspectral image contains a large amount of information, and the efficient and accurate identification of an investigative region and spectral bands containing the most information is mandatory to ensure the correct application of subsequent image analysis methods. Therefore, the first processing step involved the manual selection of a rectangular region of interest (ROI) of  $70 \times 17$  pixels from the subject's forehead, including only 100 bands in the spectral range 600 to 800 nm, where a large difference between spectral signatures of oxyhemoglobin and deoxyhemoglobin exists.<sup>12</sup> Furthermore, the second processing step was performed on each ROI to determine the inherent dimensionality of hyperspectral data and to separate the information from noise.<sup>13</sup> To accomplish this task, we used a minimum noise fraction (MNF) transform as modified from Green et al.<sup>14</sup> and implemented it in ENVI v5.1 software. The MNF transform consists of a succession of two principal component transformations. The first transformation consists of estimating the noise statistics from the hyperspectral data. The results are transformed data in which the noise is uncorrelated with unit variance. The second transformation is a standard principal component transformation of the noise-whitened data. The results of the MNF transform are MNF transformed images and their associated MNF eigenvalues (EV).<sup>15</sup> By examining both of these results, we empirically identified that only the first three MNF images associated with large EV ( $EV > 2$ ) contain useful information (Fig. 1). The 97 remaining MNF images with small EV ( $EV < 2$ ) were found to be dominated by noise.

As we can see in Fig. 1, the MNF image 1 contains the largest EV (EV: 179.5558) and, as a result, the largest amount of information. The following two images with smaller EV also contain sufficient information, but, when we get to MNF image 4 (EV: 1.9713), we can see that noise predominates. As a consequence, we established the intrinsic dimensionality of hyperspectral images at a value of 3. An inverse MNF transform was then run to obtain spectral bands free of noise, which were used for further data analysis.

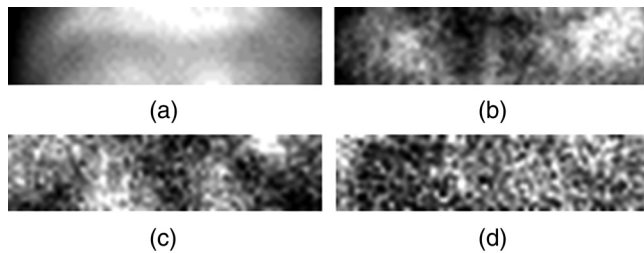


**Fig. 1** MNF images of a selected ROI from the forehead of one subject: (a) MNF image 1 (EV: 179.5558); (b) MNF image 2 (EV: 9.4659); (c) MNF image 3 (EV: 3.7541); and (d) MNF image 4 (EV: 1.9713).

## 2.5 Hyperspectral Image Analysis

The hyperspectral images, from the participants' foreheads, were analyzed for their spectral content as well as for the spatial distribution of chromophores using a spectral unmixing model based on a modified Beer-Lambert law.<sup>16</sup>

The model assumes that

- Absorbance for each pixel  $(i, j)$  in the image can be calculated as

$$A = -\log(I_{\text{calibrated}}) = -\log\left(\frac{I_{\text{subject}} - I_{\text{dark}}}{I_{\text{white}} - I_{\text{dark}}}\right). \quad (2)$$

- The main chromophores with specific absorption spectrum in the visible range that can be taken into consideration for the assessment of skin level hypoxia are oxyhemoglobin and deoxyhemoglobin. Melanin was also taken into consideration for a more accurate estimation of skin absorbance. In this case, for each pixel  $(i, j)$ , the absorbance can be estimated in accordance with a modified Beer-Lambert law

$$A(\lambda) = [\epsilon_{\text{oxy}}(\lambda) \cdot C_{\text{oxy}} + \epsilon_{\text{deoxy}}(\lambda) \cdot C_{\text{deoxy}} + \epsilon_{\text{mel}}(\lambda) \cdot C_{\text{mel}}] \cdot L + G, \quad (3)$$

where  $A(\lambda)$  is the absorbance spectrum in pixel  $(i, j)$ ,  $\epsilon_{\text{oxy}}(\lambda)$ ,  $\epsilon_{\text{deoxy}}(\lambda)$ , and  $\epsilon_{\text{mel}}(\lambda)$  represent the spectral molar extinction coefficients [ $\text{cm}^{-1}/(\text{mol}/\text{L})$ ] for oxyhemoglobin, deoxyhemoglobin, and melanin, respectively, and  $\lambda$  represents the wavelength of light. An estimate of these coefficients was done by Prahl.<sup>12</sup>  $C_{\text{oxy}}$ ,  $C_{\text{deoxy}}$ , and  $C_{\text{mel}}$  are the molar concentrations (mol/L) of the three chromophores at the pixel  $(i, j)$ , the mean path  $L$  is the average distance traveled by a photon within the tissue (cm), and  $G$  is a term that accounts for the light scattering effect at the pixel  $(i, j)$ .

To determine the oxyhemoglobin, deoxyhemoglobin, and melanin concentrations, it is necessary to know the mean path  $L$  and the way in which it changes with tissue type, wavelength, and measuring geometry.<sup>17</sup> Taking into consideration the specific measuring geometry of hyperspectral system, this is difficult to do. To overcome this difficulty, we have adopted the solution proposed by Chen et al.<sup>18</sup> who introduced a new parameter called surface molar concentration  $C^s$  [(mol/L) · cm] of chromophores, defined in each pixel  $(i, j)$  as

$$C^s = C \cdot L. \quad (4)$$

As a consequence, Eq. (3) can be written as

$$A(\lambda) = \epsilon_{\text{oxy}}(\lambda) \cdot C_{\text{oxy}}^s + \epsilon_{\text{deoxy}}(\lambda) \cdot C_{\text{deoxy}}^s + \epsilon_{\text{mel}}(\lambda) \cdot C_{\text{mel}}^s + G. \quad (5)$$

- The parameters  $C_{\text{oxy}}^s$ ,  $C_{\text{deoxy}}^s$ ,  $C_{\text{mel}}^s$ , and  $G$  in each pixel  $(i, j)$  from the image can be estimated by minimizing the sum of square difference  $\delta^2$  between the calculated absorbance data [Eq. (2)] and the estimated absorbance data described by Eq. (5) with the *nonlinear least-square* method

$$\delta^2 = \sum_k [A(\lambda_k) - \varepsilon_{\text{oxy}}(\lambda_k)C_{\text{oxy}}^S - \varepsilon_{\text{deoxy}}(\lambda_k)C_{\text{deoxy}}^S - \varepsilon_{\text{mel}}(\lambda_k)C_{\text{mel}}^S - G]^2,$$

$$\delta^2 \rightarrow \min, \quad (6)$$

where  $\lambda_k$  are the wavelength values at which the absorbance is calculated in the spectral range from 600 to 800 nm and  $k$  ranges between 1 and 100.

To perform the minimization of the  $\delta^2$  function, the authors chose the Levenberg–Marquardt algorithm<sup>19</sup> because it has the advantage of producing a more robust convergence of data. The minimization was performed using a set of initial values for the parameters specified uniquely for the whole image as follows:  $C_{\text{oxy}}^S = 5 \mu\text{mol} \cdot \text{cm}/\text{L}$ ,  $C_{\text{deoxy}}^S = 5 \mu\text{mol} \cdot \text{cm}/\text{L}$ ,  $C_{\text{mel}}^S = 0.1 \mu\text{mol} \cdot \text{cm}/\text{L}$ , and  $G = \max(A) - 1$ . The final results of the minimization process are surface molar concentrations of oxyhemoglobin  $C_{\text{oxy}}^S(i, j)$ , deoxyhemoglobin  $C_{\text{deoxy}}^S(i, j)$ , and  $C_{\text{mel}}^S(i, j)$  displayed as pseudocolor coded images.

- d. Calculated values for surface molar concentrations of oxyhemoglobin  $C_{\text{oxy}}^S(i, j)$  and deoxyhemoglobin  $C_{\text{deoxy}}^S(i, j)$  can be used to determine the oxygen saturation ( $\text{StO}_2$ ) defined as

$$\text{StO}_2 = \frac{C_{\text{oxy}}}{C_{\text{oxy}} + C_{\text{deoxy}}} = \frac{\frac{1}{L}(C_{\text{oxy}}^S)}{\frac{1}{L}(C_{\text{oxy}}^S + C_{\text{deoxy}}^S)}$$

$$= \frac{C_{\text{oxy}}^S}{C_{\text{oxy}}^S + C_{\text{deoxy}}^S}. \quad (7)$$

An algorithm for calculating all the parameters defined by the model was implemented by programs written in MATLAB software (Mathworks Inc., Natick, Massachusetts). The process of parameter calculation starts with hypercubes acquisition ( $I_{\text{subject}}$ ,  $I_{\text{dark}}$ , and  $I_{\text{white}}$ ); then, apparent absorbance  $A$  is calculated, as in Eq. (2). The starting values for  $C_{\text{oxy}}^S$ ,  $C_{\text{deoxy}}^S$ ,  $C_{\text{mel}}^S$ , and  $G$  were set to start the minimization (nonlinear least square method) procedure, as in Eq. (6). The process ends after outputting the results and the corresponding graphs. The flowchart of the algorithm is presented in Fig. 2.

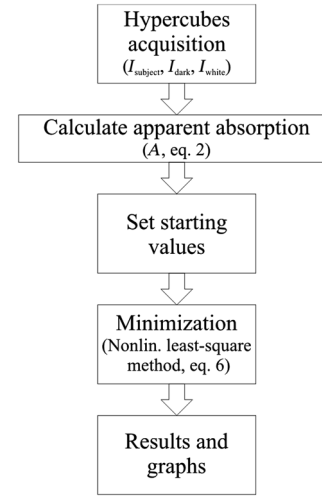


**Fig. 2** Flowchart of the algorithm for calculating the model parameters.

This unmixing model helps us to reveal the spatial distribution of oxyhemoglobin, deoxyhemoglobin, and oxygen saturation and to analyze the influence of simulated altitude on tissue oxygenation in a simple graphical manner.

## 2.6 Pulse-Oximetry Measurements

To validate the proposed model, pulse-oximetry measurements of the index finger were performed on all subjects using a pulse oximeter. We chose finger pulse oximetry because studies showed that it has a better correlation with actual arterial oxygen content than forehead pulse oximetry.<sup>20</sup> Oxygen saturation ( $\text{StO}_2$ ) was measured simultaneously with the acquisition of hyperspectral images, at the same pressure and temperature conditions.

## 2.7 Statistical Analysis

The coefficient of determination ( $R^2$ ) between the experimental and calculated values of absorbance for each pixel from the image was calculated according to Eq. (8) to assess the goodness-of-fit of nonlinear regression

$$R^2 = 1 - \frac{\sum_k^n [A(\lambda_k) - \varepsilon_{\text{oxy}}(\lambda_k)C_{\text{oxy}}^S - \varepsilon_{\text{deoxy}}(\lambda_k)C_{\text{deoxy}}^S - \varepsilon_{\text{mel}}(\lambda_k)C_{\text{mel}}^S - G]^2}{\sum_k^n \left[ A(\lambda_k) - \frac{\sum_k^n A(\lambda_k)}{n} \right]^2}, \quad (8)$$

where  $A(\lambda_k)$  represents the experimental values of absorbance at wavelength  $\lambda_k$  for a pixel  $(i, j)$ , the term  $[\varepsilon_{\text{oxy}}(\lambda_k)C_{\text{oxy}}^S + \varepsilon_{\text{deoxy}}(\lambda_k)C_{\text{deoxy}}^S + \varepsilon_{\text{mel}}(\lambda_k)C_{\text{mel}}^S + G]$  represents the calculated values of absorbance at wavelength  $\lambda_k$  for a pixel  $(i, j)$ , and  $n$  is the number of considered wavelengths. Values of  $R^2$  near 1 indicate that the calculated absorbance values are accurate.

The statistical method proposed by Bland and Altman<sup>21</sup> was used to assess the degree of agreement between the proposed HSI technique and pulse oximetry. This statistical method consists of plotting the difference between the two experimental methods against their mean. The limits of agreement were established to be between  $\Delta\text{StO}_{2\text{med}} - 2\sigma$  and  $\Delta\text{StO}_{2\text{med}} + 2\sigma$ , where  $\Delta\text{StO}_{2\text{med}}$  is the mean difference and  $\sigma$  represents the standard

deviation of the differences. These limits assure a confidence level of 95%.

## 3 Results

Figure 3 shows the distribution maps of oxyhemoglobin and deoxyhemoglobin as well as the distribution map of the coefficient of determination ( $R^2$ ) on the ROI related to the forehead of one subject calculated from hyperspectral images acquired at different time moments during hypoxia.

Figure 3(a1) shows that, before reaching the target altitude, the surface molar concentration of oxyhemoglobin is at high levels, with a maximum  $C_{\text{oxy}}^S = 42.82 \mu\text{mol} \cdot \text{cm}/\text{L}$  in the lateral sides of the forehead. At the same time, the highest

deoxyhemoglobin is found in the central area, explained probably by the territory of distribution of the supratrochlear vein [Fig. 3(b1)]. Surface molar concentration of deoxyhemoglobin is much smaller than that of the oxyhemoglobin ( $C_{\text{deoxy}}^s = 0.72 \mu\text{mol} \cdot \text{cm/L}$ ), as expected in normal saturated tissue.

After 5 min of hypoxia, the overall oxyhemoglobin concentration decreases (with a maximum of  $26.89 \mu\text{mol} \cdot \text{cm/L}$  in the same lateral area), but there is a slight increase in the central forehead [Fig. 3(a2)]. At  $t = 10 \text{ min}$ , oxyhemoglobin is uniformly decreased with a maximum in the same lateral areas of  $16.46 \mu\text{mol} \cdot \text{cm/L}$ . The concentration of deoxyhemoglobin increases at  $C_{\text{deoxy}}^s = 8.25 \mu\text{mol} \cdot \text{cm/L}$  and  $C_{\text{deoxy}}^s = 7.16 \mu\text{mol} \cdot \text{cm/L}$  (maxima in the central forehead), showing a good sensitivity of the experimental method.

The postexposure oxygen breathing for 10 min led to an increase in oxyhemoglobin and a decrease in deoxyhemoglobin, as displayed in Figs. 3(a4) and 3(b4), again most visible in the temporal areas probably due to artery distribution (the distribution is identical with the pre-experimental one). The maximal oxyhemoglobin value was  $C_{\text{oxy}}^s = 46.60 \mu\text{mol} \cdot \text{cm/L}$  and the deoxyhemoglobin value was  $C_{\text{deoxy}}^s = 1.04 \mu\text{mol} \cdot \text{cm/L}$ . The oxyhemoglobin value is higher than in the normal prehypoxia state due to enriched oxygen breathing and is correlated with a 100% reading on the pulse oximeter. The deoxyhemoglobin value is also higher, probably due to the metabolic changes in surrounding tissues, which shifted the dissociation curve.

The accuracy of the proposed unmixing model was estimated by analyzing the  $R^2$  values. As shown in Fig. 3(c1)–3(c4), a high degree of correlation was observed between experimental and calculated data with  $R^2$  values ranging from 0.9758 to 0.9823. These  $R^2$  values (relatively close to 1) indicate a

goodness of fit of regression; therefore, the model can be considered accurate enough for the determination of oxyhemoglobin and deoxyhemoglobin concentrations in skin tissue.

Using the values of surface molar concentrations of oxyhemoglobin and deoxyhemoglobin thus calculated in each pixel of hyperspectral images acquired at different time moments during the exposure, distribution maps of oxygen saturation ( $\text{StO}_2$ ) were obtained (Fig. 4).

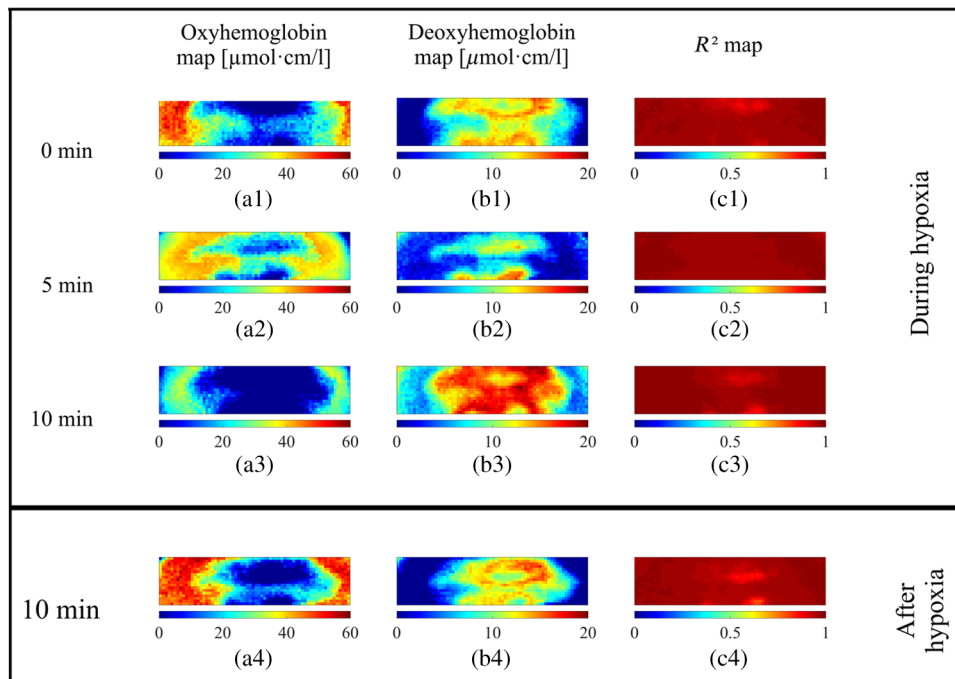
The evolution of oxygen saturation is similar to that of deoxyhemoglobin concentration, with decreases after oxygen deprivation (but a local increase in the central forehead at  $t = 5 \text{ min}$ ) and a total recovery after breathing a highly concentrated oxygen gas mixture.

Figure 5 shows good correlation between oxygen saturation values obtained from the fingers of the subjects by the pulse oximetry method and oxygen saturation values derived from the hyperspectral images of the foreheads of subjects included in this study.

As we can see in Fig. 5, the mean difference is very close to 0 ( $\Delta\text{StO}_{2\text{med}} = 0.0762\%$ ) with a standard deviation of the differences of 0.5860%. Limits of agreement ( $-1.0724\%$  and  $+1.2248\%$ ) are also close enough, so we can consider that the HSI can be successfully used in experimental practice for measuring oxygen saturation.

The changes in oxygen saturation during normobaric hypoxia (from ground level up to simulated altitude of 7620 m) and postexposure oxygen breathing for each subject included in this study are presented in Fig. 6.

We notice that each subject has his own hypoxia profile, a fact also shown in Ref. 22. The highest difference was noticed in subject 1, who was further investigated to explain such a behavior.



**Fig. 3** Distribution maps of surface molar concentrations of oxyhemoglobin and deoxyhemoglobin and  $R^2$  values for the proposed unmixing model calculated from the ROI related to the forehead of one subject at different time moments during hypoxia; (a1)–(a4) distribution maps of surface molar concentrations of oxyhemoglobin at different time moments; (b1)–(b4) distribution map of surface molar concentrations of deoxyhemoglobin at different time moments; (c1)–(c4)  $R^2$  values for the proposed unmixing model.

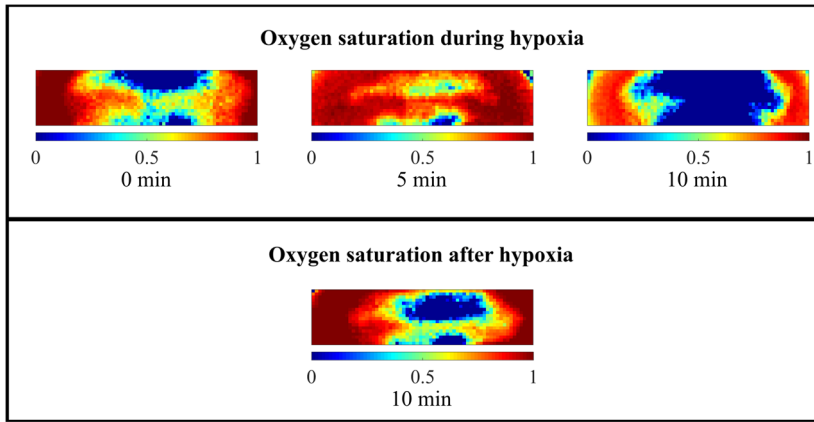


Fig. 4 Oxygen saturation maps.

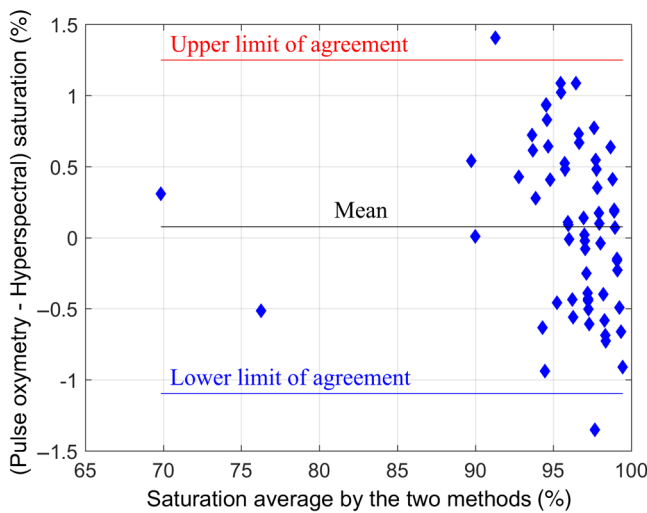


Fig. 5 Difference in the mean for oxygen saturation measured by pulse oxymetry and hyperspectral methods.

After oxygen administration, most of the observed differences were positive. Three pilots had negative differences, but they also had the lowest variation (close to zero) in oxygen saturation during the hypoxic period, demonstrating an exceptional adaptation to this situation.

#### 4 Discussion

Testing for adaptation to low oxygen pressure in inspired air is of paramount importance in the evaluation of pilots, especially in military aviation. This is done in hypobaric chambers or with a low oxygen gas mixture administered through a reduced-oxygen breathing device. Oxygen saturation is the main parameter taken into account. Pulse oximetry is usually used as the method for oxygen saturation measurement.

In this paper, a method for oxygen saturation measurement was proposed. This method consists of essentially three distinct steps: (1) hyperspectral images of the forehead acquisition, (2) hyperspectral images processing, and (3) hyperspectral images analysis using a spectral unmixing model based on a modified Beer-Lambert law. The method generates both oxyhemoglobin and deoxyhemoglobin maps and an oxygen saturation map of the investigated region. By applying this method for the simulated altitude exposure assessment, the results regarding oxygen saturation correlated well with pulse oximetry of the finger, although Self et al.<sup>22</sup> reported a higher decrease in finger oxygen saturation compared to the forehead in similar conditions.

Other studies have also reported the use of HSI to generate oxygenation maps of the skin, but the applications were diabetic foot ulcers and their behavior<sup>23</sup> or levels of oxyhemoglobin in irradiated skin.<sup>24</sup> Both groups used the same hyperspectral imager (OxyVu™, HyperMed Incorporated) and software,

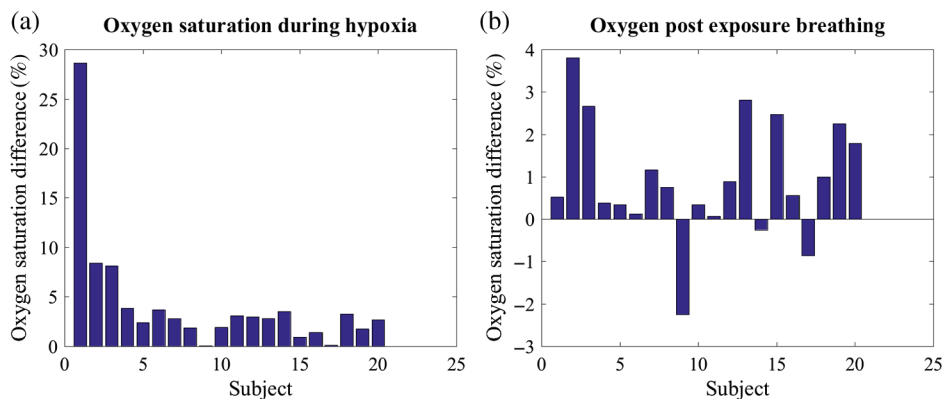


Fig. 6 Difference in oxygen saturation calculated by HSI vis-a-vis pulse-oximetry measurements: (a) normobaric hypoxia and (b) postexposure oxygen breathing.

which generates levels of oxyhemoglobin and deoxyhemoglobin in imaginary units.<sup>23</sup> The method presented in this study is able to measure hemoglobin in common units ( $\mu\text{mol} \cdot \text{cm/L}$ ).

The comparison shows that the presented method is reliable in determining oxygenation in various clinical settings. It has the ability to generate maps that can bring new insights into vascular distribution patterns in stressful conditions (like low oxygen breathing pressure). It showed that, initially, after reaching the experimental altitude, there is a slight increase in blood oxygenation in the central areas of the forehead. As these areas are supplied from the internal carotid system, it probably demonstrates a shift toward the internal carotid in comparison to the external carotid system (lateral forehead) of the main blood flow to protect the brain from hypoxia. However, the method has its disadvantages: it does not provide real-time measurements, which is not that important in experiments and can be improved by shortening the data analysis time.

Despite these limitations, we are facing a pioneering application of HSI and a reliable method for determining levels of oxygenation of the skin. Further studies are needed to shorten the data analysis time and extend the application of the method in experiments concerning a larger skin surface, which can benefit from the ability of the method to generate spatial distribution maps.

## 5 Conclusions

In conclusion, this preliminary study is the first study to quantify the changes in tissue oxygenation during simulated altitude hypoxia using the HSI technique. This technique generates oxyhemoglobin, deoxyhemoglobin, and oxygen saturation maps.

The study demonstrates that there are variations in blood oxygenation in different areas of the forehead during simulated altitude exposure. An interesting pattern of desaturation on the forehead was discovered during the study, showing one of the advantages of using HSI for skin oxygenation monitoring in hypoxic conditions compared with the punctual pulse-oximetry method. These results could bring new insight into the physiological response to high altitude, and the use of HSI could become a useful method for testing the flight crew.

## Disclosures

No conflicts of interest, financial or otherwise, are declared by the authors.

## Acknowledgments

This work was financed by the Romanian Ministry of Research and Innovation by means of the Research Program No. PN 16-40 01 01/2016.

## References

1. R. N. Pittman, "Oxygen transport in normal and pathological situations: defects and compensations," Chapter 7 in *Regulation of Tissue Oxygenation*, Vol. 3, pp. 1–100 Morgan & Claypool Life Science, San Rafael, California (2011).
2. R. H. Kellogg, "La pression barométrique: Paul Bert's hypoxia theory and its critics," *Respir. Physiol.* **34**(1), 1–28 (1978).
3. C. Neuhaus and J. Hinkelbein, "Cognitive responses to hypobaric hypoxia: implications for aviation training," *Psychol. Res. Behav. Manage.* **10**(7), 297–302 (2014).
4. J. W. Severinghaus and P. B. Astrup, "History of blood gas analysis. VI. Oximetry," *J. Clin. Monit. Comput.* **2**(4), 270–288 (1986).
5. D. Popescu and A. Macovei, "Experience with an expert system of on-ground hypoxia training," in *Proc. of the 12th Int. Scientific Conf.*

6. V. Kamat, "Pulse oximetry," *Indian J. Anaesth.* **46**(4), 261–268 (2002).
7. A. F. H. Goetz et al., "Imaging spectrometry for earth remote sensing," *Science* **228**(4704), 1147–1153 (1985).
8. G. Lu and B. Fei, "Medical hyperspectral imaging: a review," *J. Biomed. Opt.* **19**(1), 010901 (2014).
9. M. A. Calin et al., "Hyperspectral imaging in medical field: present and future," *Appl. Spectrosc. Rev.* **49**(6), 435–447 (2014).
10. G. Polder, W. A. M. Gerie, and D. H. Van, "Calibration and characterization of imaging spectrographs," *J. Near Infrared Spectrosc.* **11**, 193–210 (2003).
11. H. Akbari et al., "Hyperspectral imaging and quantitative analysis for prostate cancer detection," *J. Biomed. Opt.* **17**(7), 076005 (2012).
12. S. Prahl, "Optical absorption of hemoglobin," Tech. Rep., Oregon Medical Laser Center, <http://omlc.org/spectra/hemoglobin/> (1999).
13. F. Deger et al., "A sensor-data-based denoising framework for hyperspectral images," *Opt. Express* **23**(3), 1938–1950 (2015).
14. A. A. Green et al., "A transformation for ordering multispectral data in terms of image quality with implications for noise removal," *IEEE Trans. Geosci. Remote Sens.* **26**(1), 65–74 (1988).
15. ENVI User's Guide, *Transforms: Minimum Noise Fraction Transform*, pp. 682–695, Research Systems Inc. (2004).
16. A. Sassaroli and S. Fantini, "Comment on the modified Beer–Lambert law for scattering media," *Phys. Med. Biol.* **49**(14), N255–N257 (2004).
17. S. R. Arridge, M. Cope, and D. Delpy, "The theoretical basis for the determination of optical pathlengths in tissue: temporal and frequency analysis," *Phys. Med. Biol.* **37**, 1531–1560 (1992).
18. T. Chen et al., "Detection of psychological stress using a hyperspectral imaging technique," *IEEE Trans. Affective Comput.* **5**(4), 391–405 (2014).
19. D. W. Marquardt, "An algorithm for least-squares estimation of non-linear parameters," *J. Soc. Ind. Appl. Math.* **11**(2), 431–441 (1963).
20. S. W. Sun et al., "Reliability of forehead pulse oximetry in critically ill patients," *Chest* **124**, 178S (2003).
21. J. M. Bland and D. G. Altman, "Statistical methods for assessing agreement between two methods of clinical measurement," *Lancet* **1**(8476), 307–310 (1986).
22. D. A. Self et al., "Physiological determinants of human acute hypoxia tolerance," Tech. Rep., Civil Aerospace Medical Institute and Federal Aviation Administration 2013, [www.faa.gov/go/oamtechreports](http://www.faa.gov/go/oamtechreports).
23. D. Yudovsky, A. Nouvong, and L. Pilon, "Hyperspectral imaging in diabetic foot wound care," *J. Diabetes Sci. Technol.* **4**(5), 1099–1113 (2010).
24. M. S. Chin et al., "Hyperspectral imaging for early detection of oxygenation and perfusion changes in irradiated skin," *J. Biomed. Opt.* **17**(2), 026010 (2012).

**Mihaela Antonina Calin** received her PhD in physics from the University of Bucharest, Faculty of Physics, Romania. She is a senior researcher and head of the Optoelectronics Methods for Biomedical Applications Department at the National Institute of Research and Development for Optoelectronics—INOE 2000, Bucharest, Romania. Her research activities are mainly focused on the development of new optical diagnostic and therapeutic methods based on the interaction of laser radiation with biological tissues.

**Adrian Macovei** received his PhD in medicine from Craiova University of Medicine and Pharmacy. He is an assistant lecturer in Craiova University of Medicine and Pharmacy, Craiova, Romania, and section chief at the National Institute of Aerospace Medicine, Bucharest, Romania. He specializes in aerospace and hyperbaric medicine, and his main research focus is on human body adaptation to extreme environments.

**Sorin Miclos** is a senior researcher at the National Institute of Research and Development for Optoelectronics—INOE 2000, Bucharest, Romania. His research activities are mainly focused on the development of data processing methods for hyperspectral imaging and fiber-optics devices for medical instrumentation.

**Sorin Viorel Parasca** received his PhD from Ovidius University in Constanta, Romania. He is an assistant lecturer in plastic surgery at Carol Davila University of Medicine and Pharmacy, Bucharest,

Romania, and a consulting surgeon (plastic surgery) at the Clinical Emergency Hospital for Plastic Surgery and Burns, Bucharest, Romania. Beginning in 2005, he started a close collaboration with researchers from the National Institute of Research and Development for Optoelectronics—INOE 2000 on applications of optical physics in medicine.

**Roxana Savastru** received her PhD in technical sciences from Politehnica University of Bucharest, Romania. She is a senior researcher and general director of the National Institute of Research and Development for Optoelectronics, Romania. Her main activities are focused in the field of application, a scientific management for

improving research activity, modernization of equipment, technological design, and implementation of optomechanical systems with applications in optoelectronic diagnostic techniques, environment, industry, and art conservation.

**Razvan Hristea** is the general director and head of the Aeromedical Center at the National Institute of Aerospace Medicine, Bucharest, Romania. He specializes in general surgery and in aerospace medicine. He is the president of the Romanian Society of Aerospace Medicine. His main research focus is on optimizing human performance in the aeronautical and spatial environments, as well as selection and training of aviation and space professionals.